Optics Communications 407 (2018) 327–332

Contents lists available at ScienceDirect

Optics Communications

journal homepage: www.elsevier.com/locate/optcom

Simulating the spiking response of VCSEL-based optical spiking neuron

Qiang Li [a], Zhi Wang [a,*], Can Cui [a], Runquan Li [a], Ying Li [a], Biao Liu [b], Chongqing Wu [a]

[a] Institute of Optical Information, Key Laboratory of Luminescence and Optical Information, Ministry of Education, Beijing Jiaotong University, Beijing 100044, China
[b] School of Electrical Engineering, Beijing Jiaotong University, Beijing 100044, China

ARTICLE INFO

Keywords:
Nonlinear optics
Devices
Vertical cavity surface emitting laser
Optical processing devices

ABSTRACT

Based on the Yamada model and rate equation model of vertical cavity surface emitting laser (VCSEL) with a saturable absorber (SA), we numerically simulate the spiking response of VCSEL–based optical spiking neuron under incoherent and coherent perturbations, respectively. First, we simply analyze the dynamics of the laser system based on the Yamada model. Then we discuss the dependence of spiking characteristics, including threshold, response time, response spike's amplitude and pulse-width, with the amplitude of perturbations, the driving current of gain and SA region for single optical pulse injection. Finally, we study the dependence of relative refractory period of VCSEL-based optical spiking neuron with different amplitudes of perturbations. Since VCSELs are ease of integration, it provides new opportunities for realization of large-scale and ultrafast neuromorphic computing systems.

1. Introduction

Neuromorphic engineering, developed by Carver Mead in the late 1980s [1], aims at emulating the neurons and synapses in human brain and mimicking the behavior of human brain, and it has a wide range of applications in the fields of machine learning, pattern recognition, adaptive control, etc. The Spiking Neural Networks (SNNs), touted to be the third generation of neural network models, are one of the most popular neural network models, and the SNNs employ spiking neurons as computational units which encode information in spike trains [2]. Recently, various hardware emulations on the neuromorphic computing have been developed in very-large-scale integration (VLSI) systems, including IBM's TrueNorth chip as part of DARPA's SyNAPSE program [3], Neurogrid system as part of Stanford's Brains in Silicon program [4], the Heidelberg HICANN chip as part of BrainScaleS project [5], etc. Microelectronic SNNs are both fast and highly interconnected, but they are subject to a fundamental bandwidth connection-density tradeoff, keeping their speed limited.

In contrast, photonics, characterized by its high speed, wide bandwidth, low power consumption and high parallelism, is an ideal way to realize ultrafast spiking-based information schemes. In the last six years, some bulky optical systems have been realized [6–9], which are difficult to implement large-scale optical SNNs. Using a single optical device which is excitable is a better way to implement large-scale SNNs. The definition of excitability in physiology is that a system is excitable if it is capable to generate a large-amplitude action potential when the input perturbation is strong enough, then it will return to its initial state. Excitability have been investigated in lasers with saturable absorber (SA) [10–15], lasers with optical injection [16–23] or optical feedback [24,25], silicon-on-insulator (SOI) microrings [26], semiconductor photonic-crystal nanolaser [27].

Compared with other realizations of spiking neurons, vertical cavity surface emitting lasers (VCSELs) exhibit attractive advantages, including low cost, low power energy consumption, low threshold currents and ease of integration. Various types of optical spiking neurons have been developed by using VCSELs based on Q-switching [14,15], polarization switching [17–22] and phase modulation [23]. And VCSEL with a SA shows rich features that can better mimic the spiking neuron.

In this paper, based on the Yamada model [28], we numerically simulate the spiking response of an optical spiking neuron consisting of a VCSEL with an intra-cavity SA with optical injection. We focused on the spiking response of the laser system with incoherent perturbations, which means the wavelength of the injected optical perturbations is different from the lasing wavelength, or coherent perturbations, which means the wavelength of the injected optical perturbations is the same as the lasing wavelength. In Section 2, we simply analyzed the excitability theory of the laser system based on the Yamada model. In Sections 3 and 4, we studied the spiking characteristics under incoherent and coherent perturbations, respectively.

* Corresponding author.
E-mail address: zhiwang@bjtu.edu.cn (Z. Wang).

https://doi.org/10.1016/j.optcom.2017.09.066
Received 20 July 2017; Received in revised form 18 September 2017; Accepted 21 September 2017
Available online 5 October 2017
0030-4018/

2. Excitability theory

Laser with a SA can behave the third type optical excitability and can be described by the Yamada model as Eq. (1) [29,30].

$$\begin{aligned} \dot{G} &= \gamma_G (A - G - GI) \\ \dot{Q} &= \gamma_Q (B - Q - aQI) \\ \dot{I} &= \gamma_I (G - Q - 1) I \end{aligned} \tag{1}$$

where G is the gain, Q is the absorption, I is the laser intensity, A is the bias current of the gain, B is the level of absorption, a describes the differential absorption relative to the differential gain, γ_G and γ_Q are the relaxation rate of the gain and SA, respectively, γ_I is the reverse photon lifetime. γ_I is much larger than γ_G and γ_Q, so the Yamada model is a slow–fast system. The dynamics and bifurcations of this system were studied in Ref. [29].

In this paper, we study a laser system with spontaneous emission $\varepsilon f(G)$, which is very small and is not capable of exciting the system by itself. γ_Q and γ_G are both small, but γ_Q is much larger than γ_G. The dynamical system behaves some different characteristics compared with Ref. [29], which are much suitable to mimic the spiking neuron.

The curve $B(a-1)=1$ approximates to separate (A, γ) plane in type 1 and type 2, as illustrated in Fig. 1(a) and (b), respectively. γ is γ_G or γ_Q. For $B(a-1) < 1$, the (A, γ) plane is separated by a line T given by $A_T = B + 1$. If $A<A_T$ (region 1), $G \approx A$, $Q \approx B$, $I \approx 0$ is the only stable equilibrium, which is an attractor. If $A > A_T$ (region 9), $(A, B, 0)$ is unstable, and there is another stable equilibrium $(A/(1+I_+), B/(1+aI_+), I_+)$. For $B(a-1) > 1$, the (A, γ) plane is separated by a line T and a line S given by $A_S = \left(a - 1 + 2\sqrt{(a-1)B} + B\right)/a$. If $A < A_S$ (region 1), $(A, B, 0)$ is the only stable equilibrium. If $A_S < A < A_T$ (region 2), there are a stable equilibrium $(A, B, 0)$, and two unstable equilibriums $(A/(1+I_\pm), B/(1+aI_\pm), I_\pm)$. If $A > A_T$ (region 7 and 9), there are an unstable equilibrium $(A, B, 0)$, and a stable equilibrium $(A/(1+I_+), B/(1+aI_+), I_+)$. Where

$$I_\pm = \frac{aA - a - B - 1 \pm \sqrt{(aA - a - B - 1)^2 + 4a(A - B - 1)}}{2a}. \tag{2}$$

In region 7, the laser works as a passive mode-locked laser, which will output periodic spike trains. In region 9, the laser works as a solitary laser without SA which will output CW light. To mimic the spiking neuron, we only care about region 1 and 2. The sketch phase portraits of (G, I) plane of region 1 and 2 are shown in Fig. 2.

In regions 1 and 2, if we push the G above the threshold, which is near $G - Q - 1 > 0$, since γ_I is much larger than γ_G and γ_Q and the laser system exists spontaneous emission, the system will produce a single pulse and relax slowly back to the attractor $(A, B, 0)$.

In region 1, since γ_I and γ_Q are much larger than γ_G, if we push I above the equilibrium, I will increase fast, Q will decrease fast, and G will decrease slowly, which will make $G - Q - 1 > 0$, and I will continue increasing until $G - Q - 1 < 0$. If we push I above the threshold, the system will produce a single pulse. In region 2, if we push I above the stable manifold, the system will produce a single pulse [30].

Therefore, the laser system can be excitable by tuning G or I in regions 1 and 2, which also means it can behave excitability in both type 1 and type 2 of (A, γ) plane. In this paper, we focused on type 2 of (A, γ) plane, since it features all possible dynamics of the laser system. In the initial state, the laser is not lasing. When a sufficient high perturbation, which is incoherent or coherent, is injected into the laser, it can bring I or G above the lasing threshold, and a pulse is generated. G can be modulated by injecting incoherent perturbations θ_G, which is used for pumping the laser system, as shown in Eq. (3a), and I can be modulated by injecting coherent perturbations θ_I, as shown in Eq. (3b).

$$\dot{G} = \gamma_G (A - G - GI) + \theta_G \tag{3a}$$

$$\dot{I} = \gamma_I (G - Q - 1) I + \varepsilon f(G) + \theta_I. \tag{3b}$$

Table 1
The parameters of the simulation.

Parameters	Gain region	SA region
Cavity volume V	9.6×10^{-18} m^3	2.4×10^{-18} m^3
Confinement factor Γ	0.06	0.05
Carrier lifetime τ	1 ns	150 ps
Differential gain/loss g	2.9×10^{-12} m^3 s^{-1}	14.5×10^{-12} m^3 s^{-1}
Transparency carrier density n_0	1.1×10^{24} m^{-3}	0.89×10^{24} m^{-3}

The rate equation model of VCSELs for the total photon number N_{ph}, and the number of carriers in gain region n_a and in SA region n_s is described in Eq. (4) [13,14].

$$\begin{aligned} \dot{N}_{ph} &= \Gamma_a g_a (n_a - n_{0a}) N_{ph} + \Gamma_s g_s (n_s - n_{0s}) N_{ph} \\ &\quad - \frac{N_{ph} - \varphi_{ph}(t)}{\tau_{ph}} + V_a \beta B_r n_a^2 \\ \dot{n}_a &= -\Gamma_a g_a (n_a - n_{0a}) \frac{N_{ph} - \varphi_a(t)}{V_a} - \frac{n_a}{\tau_a} + \frac{I_a}{eV_a} \\ \dot{n}_s &= -\Gamma_s g_s (n_s - n_{0s}) \frac{N_{ph}}{V_s} - \frac{n_s}{\tau_s} + \frac{I_s}{eV_s} \end{aligned} \tag{4}$$

where e is the electron charge, I_a is the drive current of gain region, and I_s is the drive current of SA region, τ_{ph} is the photon lifetime, β is the spontaneous emission coupling factor, and B_r is the bimolecular recombination term. Other parameters are shown in Table 1. And The subscripts a and s identify the gain and SA region, respectively. $\varphi_a(t)$ represents the injected incoherent optical perturbations which only affects the carriers in the gain region and represents the optical pumping for VCSEL, and $\varphi_{ph}(t)$ represents the injected coherent optical perturbations which mainly affects the photon number in the cavity. For ease of understanding, Eq. (4) can be rewritten in dimensionless form as Eq. (1), as shown in Eq. (5).

$$\begin{aligned} G &= \tau_{ph}\Gamma_a g_a (n_a - n_{0a}), \quad Q = \tau_{ph}\Gamma_s g_s (n_{0s} - n_s) \\ I &= \frac{\tau_a \Gamma_a g_a}{V a} N_{ph}, \quad \tilde{t} = \frac{t}{\tau_{ph}}, \gamma_I = 1 \\ \gamma_G &= \frac{\tau_{ph}}{\tau_a}, \quad A = \tau_{ph}\tau_a\Gamma_a g_a \left(\frac{I_a}{eV_a} - \frac{n_{0a}}{\tau_a}\right) \\ \gamma_Q &= \frac{\tau_{ph}}{\tau_s}, \quad B = \tau_{ph}\tau_s\Gamma_s g_s \left(\frac{n_{0s}}{\tau_s} - \frac{I_s}{eV_s}\right) \\ a &= \frac{\tau_s \Gamma_s g_s V_a}{\tau_a \Gamma_a g_a V_s}, \quad \varepsilon f(G) = \tau_{ph}\tau_a\Gamma_a g_a \beta B_r n_a^2 \\ \theta_G(t) &= \frac{\tau_{ph}\Gamma_a g_a}{V_a}\varphi_a(t), \quad \theta_I(t) = \frac{\tau_a \Gamma_a g_a}{V_a}\varphi_I(t). \end{aligned} \tag{5}$$

The output power can approximate to Eq. (6) [14].

$$P_{out} \approx \frac{\eta_c \Gamma_a}{\tau_{ph}} \frac{hc}{\lambda} N_{ph} \tag{6}$$

where η_c is the output power coupling coefficient, c is the speed of light, λ is the lasing wavelength of VCSEL, and h is the plank constant.

3. Incoherent perturbations

A 1550 nm VCSEL with an intra-cavity SA was considered in this paper, and the device parameters are shown in Table 1 [13,14]. And $\tau_{ph} = 4.8$ ps, $\beta = 1\times10^{-4}$, $B_r = 10\times10^{-16}$ m^3 s^{-1}, $\eta_c = 0.4$. Then we know that $a = 2.5$, which is fixed in this paper, and the laser system works in type II of (A, γ) plane. In this section, we considered the incoherent perturbations with the wavelength of 980 nm.

3.1. Single pulse injection

To begin with, we discuss the spiking response on the amplitude of input perturbation with a single pulse. First, we set the drive current of gain and SA region as $I_a = 8.5$ mA, $I_s = 0$ mA, so $A = 3.7032$, $B = 3.0972$, $A_S = 3.5632$, $A_T = 4.0972$. Therefore, the laser system works in region 2 of (A, γ) plane. The input pulse's full width at half maximum (FWHM) $t_{fwhm} = 20$ ps, which is shorter than the relaxing time of gain region and SA region, and it was injected at $t = 1$ ns. Fig. 3 illustrates the output of the VCSEL. When the amplitude of input pulse is less than 162.21 μW, no spike is generated. When the amplitude is greater than 162.21 μW, one spike is generated quickly. As the amplitude

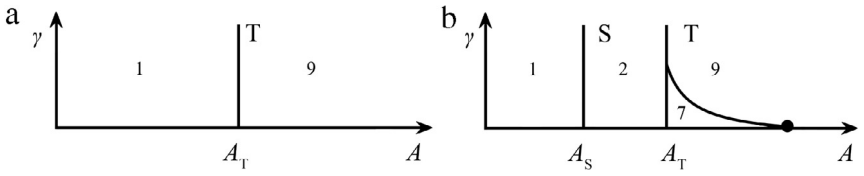

Fig. 1. Sketch of (A, γ) plane of (a) type 1 when $B(a-1) < 1$ and (b) type 2 when $B(a-1) > 1$.

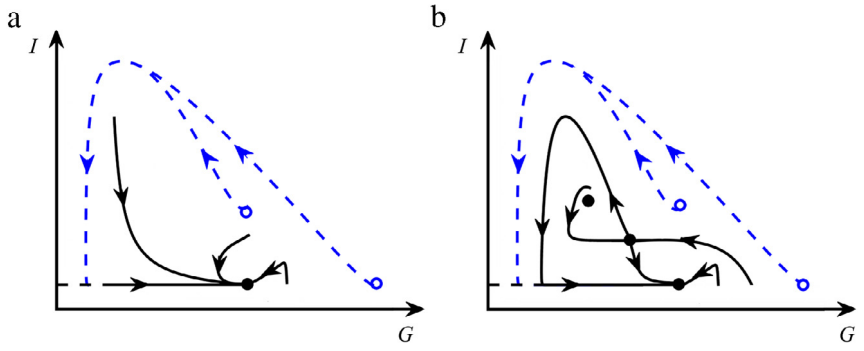

Fig. 2. Sketch of (G, I) phase portraits of (a) region 1 and (b) region 2.

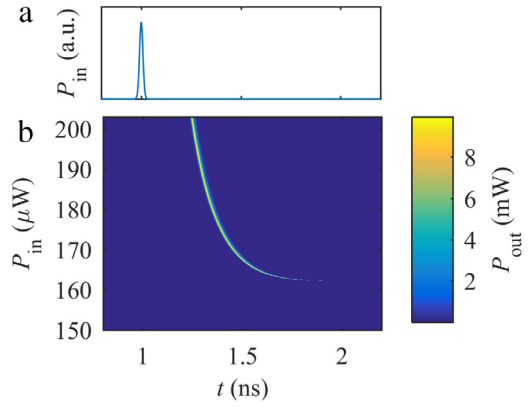

Fig. 3. (b) Temporal map of response spike's amplitude under (a) single incoherent perturbation injection with different amplitude.

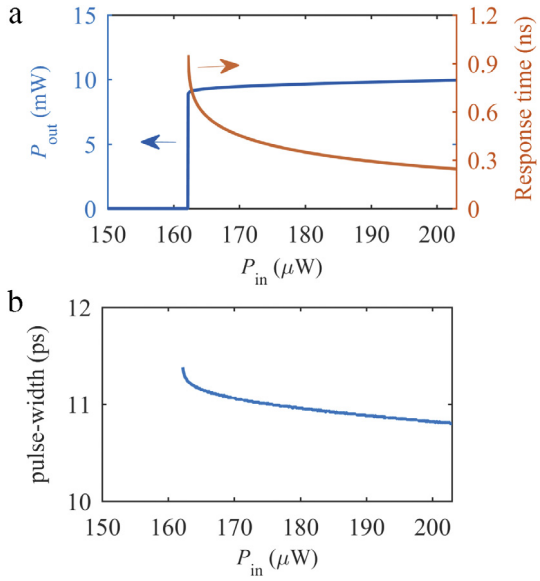

Fig. 4. The response spike's (a) amplitude and response time, and (b) pulse-width depending on the amplitude of incoherent perturbation.

increases, the response time, defined as the delay time between the input perturbation and output spike, decreases since the VCSEL is much quicker to get the threshold with larger amplitude of perturbation, as seen in Fig. 4(a), and the pulse-width of response spike first decreases because with larger amplitude of perturbation I will reach its maximum value more quickly, and then it remains almost constant since when the perturbation pushes G above the threshold, the remaining perturbation will have little effects on the response which means it will not push G far away from the threshold point, as shown in Fig. 4(b).

Then we tune the pulse-width of injection pulse from 20 ps to 60 ps, as indicated by Fig. 5. The larger pulse-width, the lower amplitude of injection pulse and response time are required to generate a spike output, as shown in Fig. 5(a) and (b), respectively, because the same amplitude with larger pulse-width means the larger perturbation energy.

In Eq. (1), A and B can be modulated by tuning the drive current of gain and SA region, respectively, so the laser system can work in different regions. First, we set $I_s = 0$ mA, $t_{fwhm} = 20$ ps. We tune I_a from 7.6 mA to 8.7 mA, which corresponds to A from 3.2138 to 3.8119. The dynamic of the laser system crosses the S line ($A_S = 3.5632$), etc. moves from region 1 to region 2. The output of the laser system is shown in Fig. 6(a). Then, we set $I_a = 7.6$ mA, etc. $A = 3.2138$. We tune I_s from 0 mA to 0.5 mA, which corresponds to B from 3.0972 to 2.4175. As indicated by Fig. 7, for $I_s < 0.37$ mA, the laser system works in region 1; for $I_s > 0.37$ mA, the laser system works in region 2. As I_a or I_s increases, the threshold almost decreases linearly since A is getting closer to A_T which means it is easier to make $G - Q - 1 > 0$, as shown in Fig. 6(a) and (b). The results show that the spiking response of the laser system by tuning G is almost the same in region 1 and region 2.

3.2. Two pulse injection

Refractory period is the recovery time of an excitable system after responding to a first perturbation, then the system will return back to its initial state slowly. There are two kinds of refractory period. The first one is the absolute refractory period, which means no response occurs in this occasion. There is no absolute refractory period in the VCSEL-based optical spiking neuron [14]. The second one is relative refractory

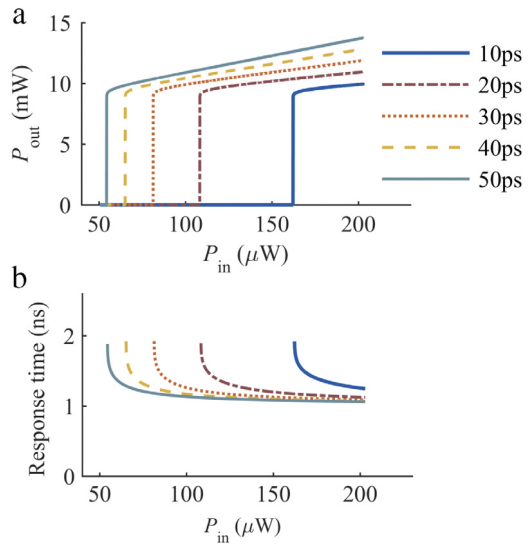

Fig. 5. (a) The response spike's amplitude and (b) response time depending on the amplitude and pulse-width of incoherent perturbation.

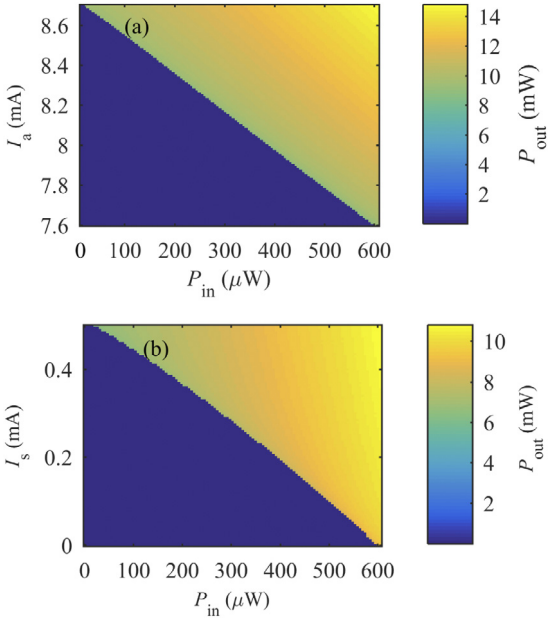

Fig. 6. The response spike's amplitude depending on the amplitude of incoherent perturbation with different (a) I_a and (b) I_s.

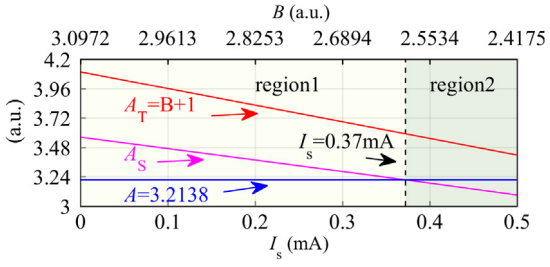

Fig. 7. The dynamic of laser system for different I_s.

period, which means a spike can be generated for a sufficiently high perturbation. In order to measure the relative refractory period of VCSEL-based optical spiking neuron, we perturb VCSEL with two optical pulses in this section.

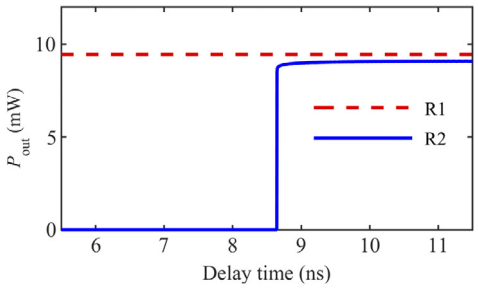

Fig. 8. The response to the first (R1, red) and second (R2, blue) perturbation for two incoherent perturbations with variable delays.

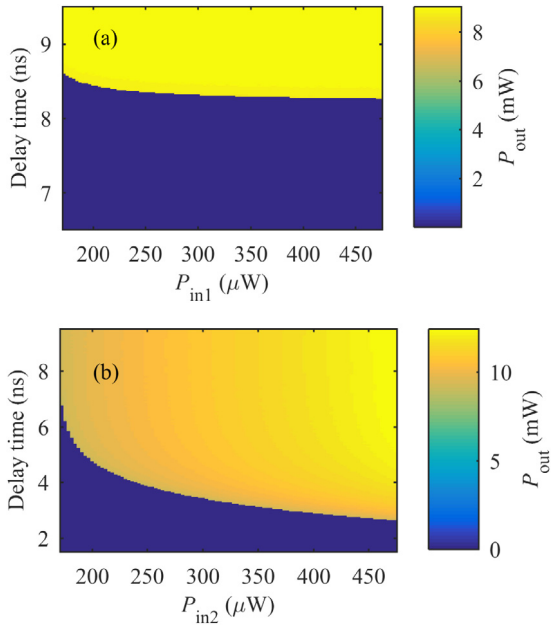

Fig. 9. Temporal map of response spike's amplitude under two incoherent perturbations with variable delays and different amplitude of (a) first pulse and (b) second pulse.

First, we set I_a = 8.5 mA, I_s = 0 mA, t_{fwhm} = 20 ps. The two injection pulses are in the same amplitude, 162.21 μW, which properly reaches the threshold. The first spike is injected at t_1 = 1 ns, and the second spike is injected from t_2 = 6.5 ns to t_2 = 12.5 ns. Fig. 8 shows the response to the first (R1) and second (R2) perturbation. The second spike will be generated if the delay time is larger than 8.65ns. In this case, the relative refractory period of the spiking neuron is about 8.65ns.

Then, we set the amplitude of the second pulse P_{in2} at 162.21 μW, and change the amplitude of the first pulse P_{in1} from 162.21 μW to 473.91 μW. As P_{in1} increases, the system will cost less time to get back to its initial state, therefore the minimize delay time required to generate the second response decreases, but it is almost constant, as seen in Fig. 9(a). At last, we set P_{in1} = 162.21 μW, and change P_{in2} from 162.21 μW to 473.91 μW. As P_{in2} increases, it is much easier to reach the threshold, so the minimize delay time required to generate the second response decreases, which means the refractory time decreases, as seen in Fig. 9(b).

4. Coherent perturbations

Coherent perturbations are important to demonstrate cascadability in neural systems, such as the feedback to the neuron itself. In this section, we will discuss the coherent perturbation with the wavelength of 1550 nm.

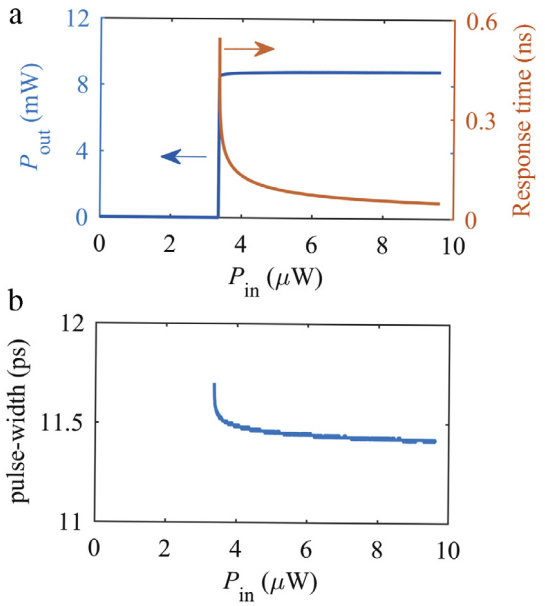

Fig. 10. The response spike's (a) amplitude and response time, and (b) pulse-width depending on the amplitude of coherent perturbation.

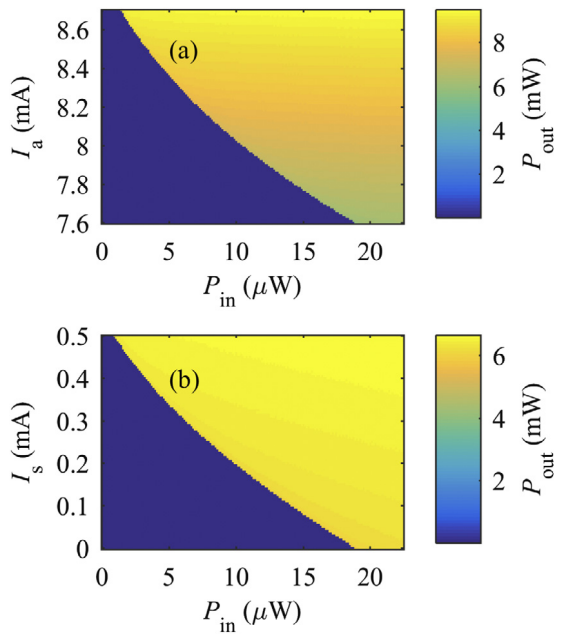

Fig. 11. The response spike's amplitude depending on the amplitude of perturbation's amplitude with different (a) I_a and (b) I_s.

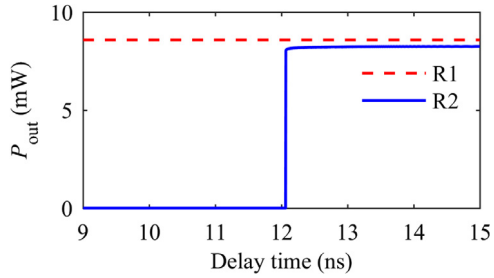

Fig. 12. The response to the first (R1, red) and second (R2, blue) perturbation for two coherent perturbations with variable delays.

4.1. Single pulse injection

To begin with, we discuss the spiking response on a single coherent perturbation with 20 ps pulse-width. We set $I_a = 8.5$ mA, $I_s = 0$ mA. Fig. 10(a) shows the excitability threshold of VCSEL-based optical spiking neuron (blue line). Since τ_{ph} is much faster than τ_a and τ_s, the coherent perturbation changes I quicker than the incoherent perturbation changes G. Therefore, the threshold of coherent perturbation is much smaller than the incoherent perturbation illustrated in Fig. 4(a). When the amplitude of perturbation is less than 3.38 μW, no spike is generated. When the amplitude is greater than 3.38 μW, one spike is generated quickly. As the amplitude increases, the response time decreases since the laser system is much quicker to reach the threshold with larger amplitude of perturbation, as shown in Fig. 10(a). The pulse-width of response spike first decreases because with larger amplitude of perturbation I will reach its maximum value more quickly, and then it remains almost constant since when the perturbation pushes I above the threshold, the remaining perturbation will have little effects on the response which means it will not push I far away from the threshold point, as shown in Fig. 10(b).

By tuning I_a and I_s, the laser system can work in different regions. First, we set $I_s = 0$ mA, $t_{fwhm} = 20$ ps. We tune I_a from 7.6 mA to 8.7 mA, which corresponds to A from 3.2138 to 3.8119, and the dynamic of the laser system crosses the S line ($A_S = 3.5632$), etc. moves from region 1 to region 2, as shown in Fig. 11(a). Then, we set $I_a = 7.6$ mA, which means $A = 3.2138$. We tune I_s from 0 mA to 0.5 mA, which corresponds to B from 3.0972 to 2.4175. As shown in Fig. 7, for I_s<0.37 mA, the laser system works in region 1; for $I_s > 0.37$ mA, the laser system works in region 2. As I_a or I_s increases, the threshold almost decreases linearly since A is getting closer to A_T and which means it is easier to reach the threshold, as seen in Fig. 11(a) and (b). The results show that the spiking response of the laser system by tuning I is almost the same in region 1 and region 2.

4.2. Two pulse injection

By perturbing the laser system with two coherent perturbations, we measure the relative refractory period. First, we set $I_a = 8.5$ mA, $I_s = 0$ mA. The two injection pulses are in the same amplitude, 3.38 μW, which properly reaches the threshold, and $t_{fwhm} = 20$ ps. The first spike is injected at $t_1 = 1$ ns, and the second spike is injected from $t_2 = 10$ ns to $t_2 = 15$ ns. Fig. 12 shows the response to the first and second perturbation. The second spike will be generated if the delay time is larger than 12.06 ns. In this case, the relative refractory period of the spiking neuron is about 12.06 ns.

5. Conclusion

In conclusion, we have numerically studied the dynamical excitability properties of VCSEL-based optical spiking neuron under incoherent and coherent perturbations. The laser system can behave excitability both in region 1 and region 2 of (A, γ) plane. There is no absolute refractory period in the laser system, but it has the relative refractory period. With the increasing amplitude of perturbation, the pulse-width and response time of response spike will decrease both under incoherent and coherent perturbations. The amplitude of perturbations required to generate a spike output under coherent perturbation is much smaller than under incoherent perturbation, which means coherent perturbation is lower power energy consumption. The threshold of the VCSEL-based optical spiking neuron can be changed through tuning the drive current of gain or SA region. Since the optical spiking neurons based on VCSELs are ease of integration, and can be integrated with optical STDP circuits [31–34], it can be used to realize large-scale and ultrafast neuromorphic computing systems.

Acknowledgment

This work was supported by National Natural Science Foundation of China (NSFC) No. 61571035, 61378061 and 61401017.

References

[1] C. Mead, M. Ismail, Analog VLSI Implementation of Neural Systems, Springer Science & Business Media, 2012.
[2] W. Maass, Networks of spiking neurons: The third generation of neural network models, Neural Netw. 10 (1997) 1659.
[3] P.A. Merolla, J.V. Arthur, R. Alvarez-Icaza, A.S. Cassidy, J. Sawada, F. Akopyan, B.L. Jackson, N. Imam, C. Guo, Y. Nakamura, A million spiking-neuron integrated circuit with a scalable communication network and interface, Sci. 345 (2014) 668.
[4] B.V. Benjamin, P. Gao, E. McQuinn, S. Choudhary, A.R. Chandrasekaran, J. Bussat, R. Alvarez-Icaza, J.V. Arthur, P.A. Merolla, K. Boahen, Neurogrid: A mixed-analog-digital multichip system for large-scale neural simulations, Proc. IEEE 102 (2014) 699.
[5] J. Schemmel, D. Briiderle, A. Griibl, M. Hock, K. Meier, S. Millner, A wafer-scale neuromorphic hardware system for large-scale neural modeling, in Proceedings of 2010 IEEE International Symposium on Circuits and Systems (2010) pp. 1947.
[6] K.S. Kravtsov, M.P. Fok, P.R. Prucnal, D. Rosenbluth, Ultrafast all-optical implementation of a leaky integrate-and-fire neuron, Opt. Express 19 (2011) 2133.
[7] M.P. Fok, H. Deming, M. Nahmias, N. Rafidi, D. Rosenbluth, A. Tait, Y. Tian, P.R. Prucnal, Signal feature recognition based on lightwave neuromorphic signal processing, Opt. Lett. 36 (2011) 19.
[8] B. Gholipour, P. Bastock, C. Craig, K. Khan, D. Hewak, C. Soci, Amorphous metal-sulphide microfibers enable photonic synapses for brain-like computing, Adv. Opt. Mater. 5 (2015) 635.
[9] B. Romeira, F. Kong, J.M.L. Figueiredo, J. Javaloyes, J. Yao, H.-S. Spiking, Bursting oscillations in a long-delayed broadband optoelectronic oscillator, J. Lightwave Technol. 33 (2015) 503.
[10] M.A. Nahmias, A.N. Tait, B.J. Shastri, T.F. de Lima, P.R. Prucnal, Excitable laser processing network node in hybrid silicon: Analysis and simulation, Opt. Express 23 (2015) 26800.
[11] F. Selmi, R. Braive, G. Beaudoin, I. Sagnes, R. Kuszelewicz, T. Erneux, S. Barbay, Spike latency and response properties of an excitable micropillar laser, Phys. Rev. E 94 (2016) 42219.
[12] S. Barbay, R. Kuszelewicz, A.M. Yacomotti, Excitability in a semiconductor laser with saturable absorber, Opt. Lett. 36 (2011) 4476.
[13] D. Nugent, R. Plumb, M.A. Fisher, D. Davies, Self-pulsations in vertical-cavity surface-emitting lasers, Electron. Lett. 31 (1995) 43.
[14] M.A. Nahmias, B.J. Shastri, A.N. Tait, P.R. Prucnal, A leaky integrate-and-fire laser Neuron for ultrafast cognitive computing, IEEE J. Sel. Top. Quant. 19 (2013) 1.
[15] S. Barbay, I. Sagnes, R. Kuszelewicz, A.M. Yacomotti, Localized states and excitability in a monolithic vcsel with saturable absorber, in: 2011 Fifth Rio De La Plata Workshop on Laser Dynamics and Nonlinear Photonics, IEEE, 2011.
[16] K. Alexander, T. Van Vaerenbergh, M. Fiers, P. Mechet, J. Dambre, P. Bienstman, Excitability in optically injected microdisk lasers with phase controlled excitatory and inhibitory response, Opt. Express 21 (2013) 26182.
[17] A. Hurtado, J. Javaloyes, Controllable spiking patterns in long-wavelength vertical cavity surface emitting lasers for neuromorphic photonics systems, Appl. Phys. Lett. 107 (2015) 241103.
[18] T. Deng, G. Xia, J. Chen, X. Tang, X. Lin, X. Yang, S. Huang, Z. Wu, Experimental investigation on nonlinear dynamics of 1550 nm VCSEL simultaneously subject to orthogonal optical injection and negative optoelectronic feedback, Laser Phys. 27 (2017) 45402.
[19] S. Xiang, A. Wen, W. Pan, Emulation of spiking response and spiking frequency property in VCSELs-based Photonic Neuron, IEEE Photonics J. 8 (2016) 1504109.
[20] J. Robertson, T. Deng, J. Javaloyes, A. Hurtado, Controlled inhibition of spiking dynamics in VCSELs for neuromorphic photonics: Theory and experiments, Opt. Lett. 42 (2017) 1560.
[21] S.Y. Xiang, H. Zhang, X.X. Guo, J.F. Li, A.J. Wen, W. Pan, Y. Hao, Cascadable Neuron-like spiking dynamics in coupled VCSELs subject to orthogonally polarized optical pulse injection, IEEE J. Sel. Top. Quant. 23 (2017) 1700207.
[22] T. Deng, J. Robertson, A. Hurtado, Controlled propagation of spiking dynamics in vertical-cavity surface-emitting lasers: Towards neuromorphic photonic networks, IEEE J. Sel. Top. Quant. 23 (2017) 1800408.
[23] B. Garbin, A. Dolcemascolo, F. Prati, J. Javaloyes, G. Tissoni, S. Barland, Refractory period of an excitable semiconductor laser with optical injection, Phys. Rev. E 95 (2017) 12214.
[24] T. Sorrentino, C. Quintero-Quiroz, A. Aragoneses, M.C. Torrent, C. Masoller, Effects of periodic forcing on the temporally correlated spikes of a semiconductor laser with feedback, Opt. Express 23 (2015) 5571.
[25] A. Aragoneses, S. Perrone, T. Sorrentino, M.C. Torrent, C. Masoller, Unveiling the complex organization of recurrent patterns in spiking dynamical systems, Sci. Rep-UK 4 (2014) 4696.
[26] T. Van Vaerenbergh, M. Fiers, P. Mechet, T. Spuesens, R. Kumar, G. Morthier, B. Schrauwen, J. Dambre, P. Bienstman, Cascadable excitability in microrings, Opt. Express 20 (2012) 20292.
[27] A.M. Yacomotti, S. Haddadi, S. Barbay, Self-pulsing nanocavity laser, Phys Rev A 87 (2013) 41804.
[28] M. Yamada, A theoretical analysis of self-sustained pulsation phenomena in narrow-stripe semiconductor lasers, IEEE J. Quantum Elect. 29 (1993) 1330.
[29] J.L. Dubbeldam, B. Krauskopf, Self-pulsations of lasers with saturable absorber: Dynamics and bifurcations, Opt. Commun. 159 (1999) 325.
[30] J.L. Dubbeldam, B. Krauskopf, D. Lenstra, Excitability and coherence resonance in lasers with saturable absorber, Phys. Rev. E 60 (1999) 6580.
[31] M.P. Fok, Y. Tian, D. Rosenbluth, P.R. Prucnal, Pulse lead/lag timing detection for adaptive feedback and control based on optical spike-timing-dependent plasticity, Opt. Lett. 38 (2013) 419.
[32] Q. Ren, Y. Zhang, R. Wang, J. Zhao, Optical spike-timing-dependent plasticity with weight-dependent learning window and reward modulation, Opt. Express 23 (2015) 25247.
[33] R. Toole, A. Tait, T. Ferreira De Lima, M. Nahmias, B. Shastri, P. Prucnal, M. Fok, Photonic implementation of spike timing dependent plasticity and learning algorithms of biological Neural systems, J. Lightwave Technol. 34 (2016) 470.
[34] Q. Li, Z. Wang, Y. Le, C. Sun, X. Song, C. Wu, Optical implementation of neural learning algorithms based on cross-gain modulation in a semiconductor optical amplifier, Proc. SPIE 10019 (2016) 100190E.